Experimental constraints on amphibole stability in primitive alkaline and calc-alkaline magmas

Barbara Bonechi [*], Cristina Perinelli, Mario Gaeta, Vanni Tecchiato, Serena F. Granati

Dipartimento di Scienze della Terra, SAPIENZA Università di Roma, P.le Aldo Moro 5, 00185 Roma, Italy

ABSTRACT

Equilibrium crystallization experiments were carried out on two primitive basaltic rocks (APR16: Na_2O+K_2O=4.40 wt%; CM42: Na_2O+K_2O=2.59 wt%) with the aim to investigate the amphibole stability in the differentiation processes at deep crustal level, of primitive alkaline (APR16) and calc-alkaline (CM42) magmas. The experiments were performed with different initial H_2O contents (0-5 wt%), at pressure of 800 MPa, in the temperature range of 975-1225 °C. For the explored conditions, amphibole crystallization occurs in both compositions at H_2O in the melt >7wt% while the temperature of their occurrence is lower in the alkaline composition (<1050 °C in APR16 and ≥1050 °C in CM42). Moreover, amphibole crystallization seems to be influenced by the Na_2O/K_2O ratio rather than the absolute Na_2O content in the melt. This is evident when experimental results on the APR16 and CM42 are compared with experimental data obtained from a primitive ultrapotassic composition (leucite-basanite: Na_2O+K_2O=4.58 wt%) and with thermodynamic modelling by the Rhyolite-MELTS algorithm. The comparison shows that amphibole never saturates the leucite-basanite at any of the investigated/modelled conditions, even when an extended crystallization increases the Na_2O of melts up to contents like those of calc-alkaline experimental glasses. We conclude that, at pressure of 800 MPa and hydrous conditions, only primitive liquids with Na_2O/K_2O ratio ≥0.9 are more prone to crystallize amphibole.

Keywords: Experimental petrology; Rhyolite-MELTS modelling; Calcic amphibole; Calc-alkaline melts; Alkaline melts; Na_2O/K_2O ratio.

INTRODUCTION

At the vast majority of volcanic arcs, the dominant erupted magma type is usually too evolved to have equilibrated directly with a mantle peridotite source at depth, suggesting that primary melts undergo significant differentiation at the roots of continental crust (Grove et al., 2003; Melekhova et al., 2015 and references therein). In this environment, high pressure and hydrous conditions favour significant amphibole crystallization, with remarkable effects on arc magmas evolution (Cawthorn et al., 1976; Hilyard et al., 2000; Müntener and Ulmer, 2006; Davidson et al., 2007; Nandedkar et al., 2014). Experimental studies have shown that amphibole crystallizes under hydrous conditions from a wide variety of liquids at crustal pressures - i.e. dacitic and andesitic magmas (Allen and Boettcher, 1983; Rutherford and Devine, 1988; Grove et al., 1997; Prouteau and Scaillet, 2003; Alonso-Perez et al., 2009; Masotta and Keppler, 2015), tholeiitic basalts (Holloway and Burnham, 1972; Helz, 1973; Anderson, 1980) and primitive magmas of arc systems (Moore and Carmichael, 1998; Blatter and Carmichael, 1998; Pichavant and MacDonald, 2007).

PM

Factors that primarily control amphibole crystallization are (i) magma water content (Holloway and Burnham, 1972; Anderson, 1980; Medard and Grove, 2008; Krawczynski et al., 2012), (ii) oxygen fugacity (i.e., ΔNNO between -0.51 and +3; Helz, 1973, 1976; Barclay and Carmichael, 2004; Krawczynski et al., 2012; Melekhova et al., 2015) and (iii) alkali content (Cawthorn and Ohara, 1976; Nandedkar et al., 2014). Cawthorn and Ohara (1976) and Nandedkar et al. (2014) denote that calc-alkaline liquids achieve amphibole saturation for $Na_2O>3$ wt%. Amphibole has been synthesised experimentally from a wide range of starting materials over a pressure range of 1-23 kbar and 400-1150 °C and therefore, it can be a considerable indicator of crystallization conditions, both as a geothermometer and geobarometer. Holland and Richardson (1979) examined equilibria among the end-member species glaucophane, edenite, tremolite, and hornblende in assemblages with chlorite, epidote, albite, quartz and H_2O in order to explain zoning profiles in amphibole as P-T-time indicators; Graham and Powell (1984) have formulated a garnet-amphibole thermometer for application to amphibolite grade metamorphic rocks; Hammarstrom and Zen (1986) and Hollister et al. (1987) have proposed an empirical amphibole geobarometer for use with granitoid rocks. Nabelek and Lindsley (1985) proposed a preliminary empirical calibration of a hornblende-plagioclase thermometer while Ridolfi et al. (2010) and Ridolfi and Renzulli (2012), relying on a large number of experimental and natural data, proposed a model requiring only the amphibole compositions to estimate the physico-chemical parameters (P, T, fO_2 and the amount of H_2O dissolved in the melt) of calcic amphibole crystallization from calc-alkaline and alkaline melts. In order to explore the influence of alkali in primitive melts on amphibole stability at deep-crustal level, we report the results of new phase equilibria experiments performed at P=800 MPa, T=975-1225 °C, on two primitive (Mg#=Mg/(Mg+Fe$_{tot}$)=0.64-0.69; with total Fe as Fe^{2+}) basaltic compositions APR16 and CM42 characterized by different amount of alkali (Na_2O+K_2O=4.40 and 2.59 wt%, respectively) and alkali ratio (Na_2O/K_2O=1.89 and 2.08 wt%, respectively). We also compare the experimental phase relations with those calculated by means of the Rhyolite-MELTS software (Ghiorso and Sack, 1995; Asimow and Ghiorso, 1998; Gualda et al., 2012) and those obtained experimentally on primitive ultrapotassic basalt by Conte et al. (2009) to discuss the stability of amphibole in primitive alkaline and subalkaline magmas.

EXPERIMENTAL AND THERMODYNAMIC APPROACH
Starting material
We selected two samples of primitive basalts with different alkali contents (Table S1) as starting material

for equilibrium experiments. APR16 is a lithic lava clast (D'Antonio et al., 1999) occurring in the deposit of the Solchiaro hydromagmatic centre located in the Procida island belonging to the Phlegraean Volcanic District (South Italy; Figure 1a). It consists in a primitive alkaline basalt (Mg#=0.64, Na_2O+K_2O=4.40 wt%, L.O.I.=0.61 wt%; Figure 2) with 12 vol% of forsteritic olivine and diopsidic clinopyroxene phenocrysts in a groundmass of olivine, clinopyroxene, plagioclase, Ti-magnetite, alkali feldspar and glass (D'Antonio et al., 1999). Inclusions of Cr-spinel can be found within olivine phenocrysts. CM42 is a mafic enclaves occurring in the calc-alkaline hypabyssal rocks of the Capo Marargiu Volcanic District (Tecchiato et al., 2015; Figure 1 b-c). The sample is a primitive calc-alkaline basalt (Mg#=0.69, Na_2O+K_2O=2.59 wt%, L.O.I.=2.50 wt%) with ~50 vol% of clinopyroxene, amphibole, plagioclase, olivine and magnetite phenocrysts in a groundmass of plagioclase, clinopyroxene, low-Ca pyroxene and magnetite (Tecchiato et al., 2015). Centimetre-sized fragments of the APR16 and CM42 samples without weathering evidences were crushed in an agate shatterbox and subsequently by hand, under acetone, in an agate mortar. We obtain a final grain-size <60 µm (as estimated through the SEM images).

Experimental procedures
We carried out experiments with different initial H_2O contents (from 0 to 5 wt%), at pressure of 800 MPa and temperatures from 975 to 1225 °C, using an end-loaded piston cylinder apparatus installed at the HP-HT Laboratory of the Earth Science Department, "Sapienza" University of Rome (Figure 3a). This device is a solid medium press equipped with a ½ inch pressure vessel (Figure 3b) capable of attaining pressure of 3.5 GPa and temperature of 1500 °C. We load Au$_{75}$-Pd$_{25}$ alloy capsules (7 mm of length and 2.8 mm of diameter) with the starting material and appropriate amounts of water (using a microsyringe) before sealing the capsule tip by arc welding.

We use an assembly as described in Figure 3d, whose components are: a) a fluorite cylinder (CaF$_2$), which converts from uniaxial to hydrostatic pressure; b) a graphite cylinder that acts as a heating furnace; c) two cylindrical supports of workable magnesia (MgO) bored to allow the insert of the thermocouple; d) a ceramic sleeve placed between the magnesia supports to prevent capsule and thermocouple to be at direct contact. The assembly is prepared placing the capsule into the MgO supports and filling the spaces with pyrophyllite powder. Pyrophyllite prevents undesired capsule movements during pressurization as well as hydrogen loss produced by water dissociation and hydrogen permeation through the capsule alloy during experimental runs. Before placing the assembly into the pressure vessel it is wrapped
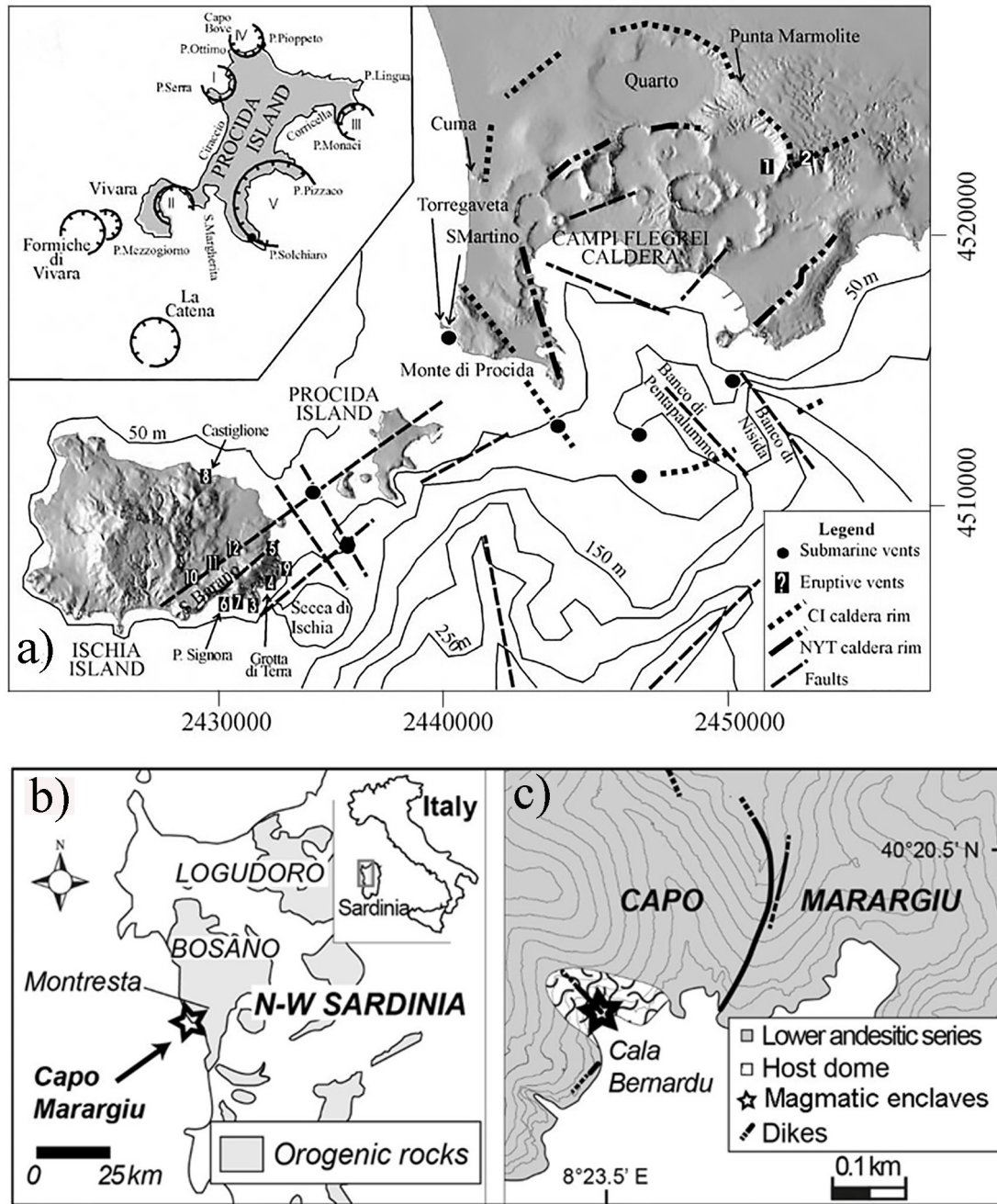
Figure 1. Sketch map of the Phlegraean Volcanic District (modified from De Astis et al., 2004), showing main tectonic structures, caldera rims and vent locations; the inset map shows an enlarged view of Procida Island and the outcrop (empty star) of the sample APR16 (a). Geological sketch map of the NW sector of Sardinia (b) and of Capo Marargiu Volcanic District (c); the black star in (c) shows the outcrop of the sample CM42.

in a lead foil; the lead foil has the function of lubricant between the assembly and the pressure vessel walls. We therefore position in-to the pressure vessel (i.e., above the assembly) a stainless-steel plug surrounded by a pyrophyllite ring; the plug acts as an electric conductor ensuring energy supply to the graphite furnace. We finally set the pressure vessel in the piston cylinder apparatus. We used an insulating mylar foil and a plexiglas support to hold the thermocouple plate above the pressure vessel. We insert a type D thermocouple (W_{97}-Re_3-W_{75}-Re_{25}) on the upper side of the plate, within a groove accurately designed for this purpose. This thermocouple
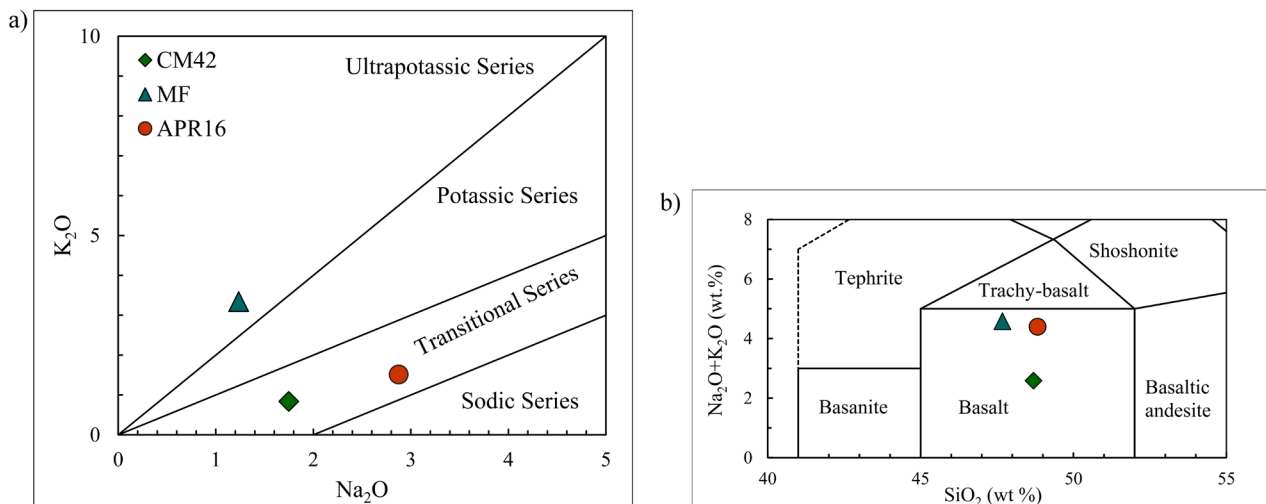
Figure 2. a) Total Alkali Silica (TAS, Le Bas et al., 1986) diagram showing the composition of primitive basalts (APR16 and CM42) used as starting materials for the experiments; b) APR16 and CM42 are plotted into the K_2O vs. Na_2O diagram which shows the fields for ultrapotassic, potassic, transitional and sodic alkaline series (Middlemost, 1975; Le Maitre, 1989). Also plotted in the diagrams is the leucite-basanite experimentally studied by Conte et al. (2009) whose results are used for comparison.

allows to monitor temperature in the isothermal zone of the assembly with accuracy of ±5 °C. At the beginning of each experiment, we achieve the working conditions of pressure and temperature using the "hot piston out" technique. This consists in (i) applying an overpressure >10% of the run pressure, (ii) gradually increasing the temperature, and (iii) correcting for pressure drops due to stress relaxation within the assembly during heating. We terminate the experimental runs after 3-6 hours; the isobaric quench was made by turning off the power.

Finally, all the runs were self-buffered; we attempt to estimate fO_2 through the equation of Kress and Carmichael (1991) using the liquid Fe^{3+}/Fe_{tot} mole ratios from K_D Fe-Mg Ol/Liq calculated according to Toplis (2005). This procedure yielded fO_2 values of ΔNNO +0.2 to +1.1, in agreement with those estimate for similar furnace assemblages (Conte et al., 2009; Weaver et al., 2013).
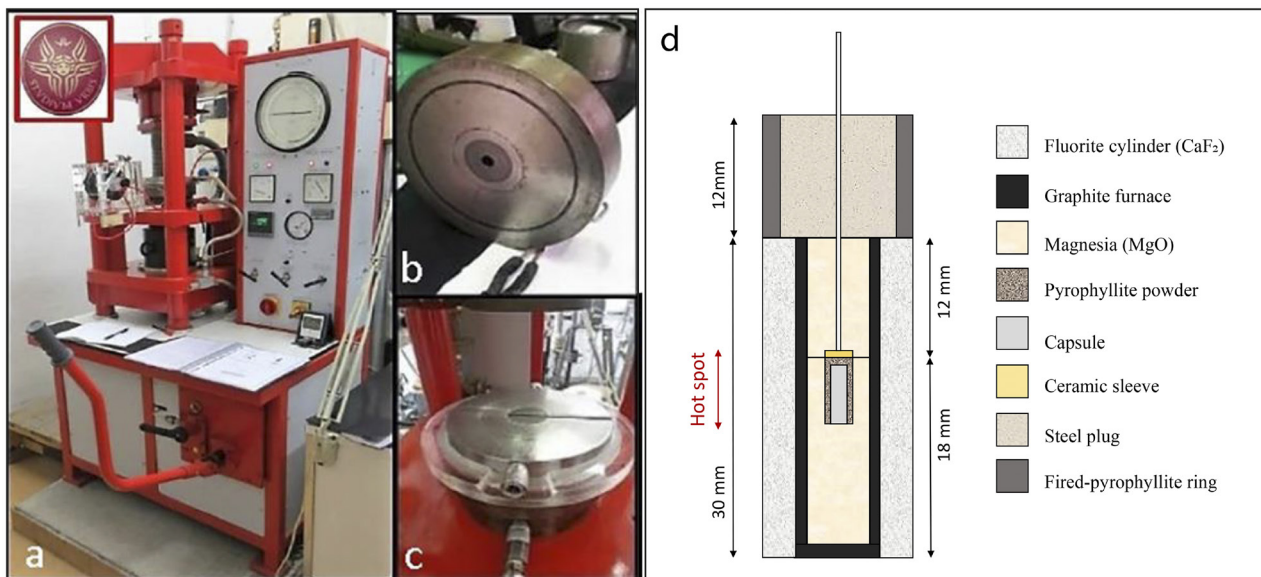
Figure 3. Piston cylinder apparatus at the HP-HT Laboratory of the Dipartimento di Scienze della Terra, SAPIENZA Università di Roma (a); ½ inch pressure vessel (b); thermocouple plate (c), cross section of the experimental assembly (d).

Analytical methods

After each experiment, we recover and mount the product in epoxy resin for polishing and carbon coating. We characterize textures and phase assemblages by Scanning Electron Microscopy (SEM) using a FEI quanta 400 equipped for microanalysis with an EDAX Genesis system at the Dipartimento di Scienze della terra, SAPIENZA Università di Roma. We estimate the modal proportion of each phase in the experimental products by detailed image analysis using ImageJ freeware (http:// imagej.nih. gov/ij/) following the procedure described by Philpotts and Ague (2009). The ease to threshold the experimental phases from SEM images yielded a good estimate of their modal abundance. We analyse phase compositions by Electron Probe Micro-Analysis (EPMA) using a Cameca SX50 equipped with five-wavelength dispersive spectrometer (WDS). The EPMA facility belongs to CNR-Istituto di Geologia Ambientale e Geoingegneria (Rome). A 15 kV accelerating voltage, 15 nA beam current and the following standards are used: metals for Mn and Cr, jadeite for Na, wollastonite for Si and Ca, orthoclase for K, corundum for Al, magnetite for Fe, rutile for Ti and periclase for Mg. Raw data are corrected using the ZAF method. We analyse minerals using a beam diameter of 1 μm, and glasses with a defocused beam from 10 to 15 μm of diameter to minimize the alkali loss. Water contents of experimental glasses are estimated according to the by-difference method (Devine et al., 1995).

Thermodynamic approach

We constrain phase equilibria at high pressure for APR16 and CM42 on a thermodynamic base using Rhyolite-MELTS (Ghiorso and Sack, 1995; Asimow and Ghiorso, 1998; Gualda et al., 2012). Similarly, we model the crystallization of a leucite-basanite (MF: Mg#=0.75, Na_2O+K_2O=4.58, L.O.I.=0.65 wt%; Table 1) from Montefiascone centre (Vulsini Volcanic District, Central Italy). This latter has been object of a previous experimental study by Conte et al. (2009). For APR16 and CM42, Rhyolite-MELTS calculations are performed at isobaric conditions (800 MPa), consistently with our phase equilibria experiments. Conversely, MF crystallization is modelled at 1000 MPa to match the experimental pressure conditions of Conte et al. (2009). Isobaric cooling simulations start at superliquidus temperatures and initial water content (H_2O_i) ranging from 0 to 7 wt%. According to the experimental study, we constrain the redox conditions of magma at the Ni-NiO (NNO) buffer.

EXPERIMENTAL AND THERMODYNAMIC MODELING
Experimental results

The phase assemblages of the run products are presented in Table 1. Experiments are always below the liquidus temperatures and, according to the occurrence of euhedral minerals, are characterized by the equilibrium between the melt and crystalline phases (Figure 4).

As regards APR16, clinopyroxene is the mineral crystallized from the NWA (no water added) run at the highest temperature (1225 °C). Olivine (Ol), oxide (Ox) and plagioclase (Plg) are obtained at 1000 °C, and K-feldspar (KFld) crystallizes at 975 °C (i.e., NWA run solidus). In the hydrous experiments (~5 wt% H_2O_i), APR16 crystallizes (i) Cpx+Ol+orthopyroxene (Opx)+Ox at 1050 °C, and (ii) Cpx+Opx+amphibole (Amph)+Ox at 1000 °C (Table 1). Remarkably, Plg never crystallizes under hydrous conditions, whereas Ol is absent at low temperature.

As regards CM42, the mineral assemblage resulting from the damp run (~2 wt% H_2O_i) at 1110 °C is Cpx+Ol+Opx+Plg+Ox. In turn, that from the wet run (~5 wt% H_2O_i) at 1050 °C is Cpx+Ol+Amph+Ox (Table 1). Notably, high water contents suppress Opx and Plg crystallization.

Phase compositions

The compositions of minerals and glasses are reported in Table S2-S7. However, both the small size of K-feldspar and of most oxides, as well as the paucity of residual glass in some runs (i.e., APR16-2C), prevent the accurate acquisition of electron microprobe analyses on these phases.

Olivines

Forsterite (Fo) content of APR16 experimental olivines in the NWA runs does not change with the decrease of temperature (Fo_{67}) while the Ol composition at hydrous conditions is Fo_{85} (Table S2). Olivines from CM42 have compositions Fo_{81} and Fo_{79} for the 2 wt% and 5 wt% H_2O_i runs, respectively (Table S2).

Pyroxenes

Clinopyroxenes in APR16 experimental sample are diopsides (Wo_{45-48}, En_{39-48}, Fs_{7-13}; Figure 5) according to the classification scheme of Morimoto et al. (1988). In the NWA runs, the Mg# decreases from 0.87 to 0.76 with temperature, whereas TiO_2 increases from 0.67 wt% at 1225 °C to 1.89 wt% at 975 °C (Table S3). In comparison, Cpx from the hydrous runs (5 wt% H_2O_i) at 1050-1000 °C shows higher Mg-number ($Mg\#_{0.81-0.82}$) and lower TiO_2 contents (1.35-1.31 wt%; Table S3). Opx is classified as clinoenstatite (Wo_5, En_{81}, Fs_{14}; Figure 5).

Experimental clinopyroxenes from CM42 runs are diopsides (Wo_{43-47}, En_{40-47}, Fs_{7-14}; Table S3). Cpx compositions from the wet run (~5 wt% H_2O_i) show lower Al_2O_3 and higher FeO contents than Cpx crystallized from the damp run (~2 wt% H_2O_i). Interestingly, the initial H_2O content of starting material does not influence Cpx Mg-

Table 1. Experimental run conditions, phase assemblages and proportions.

Run#	T (°C)	P (MPa)	Time (h)	H_2O_i	H_2O_f	Phase assemblage
APR16-35	1225	800	6	NWA	1.70	Gl (96) + Cpx (4)
APR16-2C	1000	800	3	NWA	-	Gl†(3) + Cpx (50) + Ol (10) + Plg (28) + Ox (9)
APR16-3C	975	800	3	NWA	-	Cpx (51) + Ol (10) + Plg (32) + Ox (7) ± KFld (trace) †
APR16-W7	1050	800	3	4.7	6.2	Gl (78) + Cpx (15) + Ol (5) + Opx (2) + Ox (trace) †
APR16-W13	1000	800	3	4.8	7.4	Gl (58) + Cpx (21) + Opx (1) + Amph (18) + Ox (2)
CM42-2	1110	800	3	2	4.9	Gl (42) + Cpx (23) + Ol (11) + Opx (0.2) + Plg (22.8) + Ox (1)
CM42-1	1050	800	3	5	7.1	Gl (67) + Cpx (8) + Ol (3) + Amph (21) + Ox (1)
PC185*	1275	1000	18	NWA	1.6	Gl (83.5) + Ox (0.9) + Ol (3.7) + Cpx (11.9)
PC106*	1200	970	27	3	4.3	Gl (78.6) + Ox (2) + Ol (5.2) + Cpx (14.2)
PC111*	1150	1000	70	3	5.3	Gl (54.8) + Ox (1.8) + Cpx (30.5) + Phlog (12.9)
PC108*	1200	1000	35	4	8.6	Gl (86.2) + Ox (1.2) + Ol (3.9) + Cpx (6.4) + Phlog (2.3)
PC112*	1150	1000	70	4	4.8	Gl (55.9) + Ox (0.6) + Cpx (23.8) + Phlog (19.7)

NWA = no water added; H_2O_i% of water added to the charge. H_2O_f as determined by the by-difference calculation method (respect to the total of EMP analyses).

Gl = glass; Cpx = clinopyroxene; Ol = Olivine; Plg = plagioclase; Phlog = phlogopite; Amph = amphibole; Ox = oxide; KFld = KFeldspar. † phases too small for analysis; *: data from Conte et al., 2009.
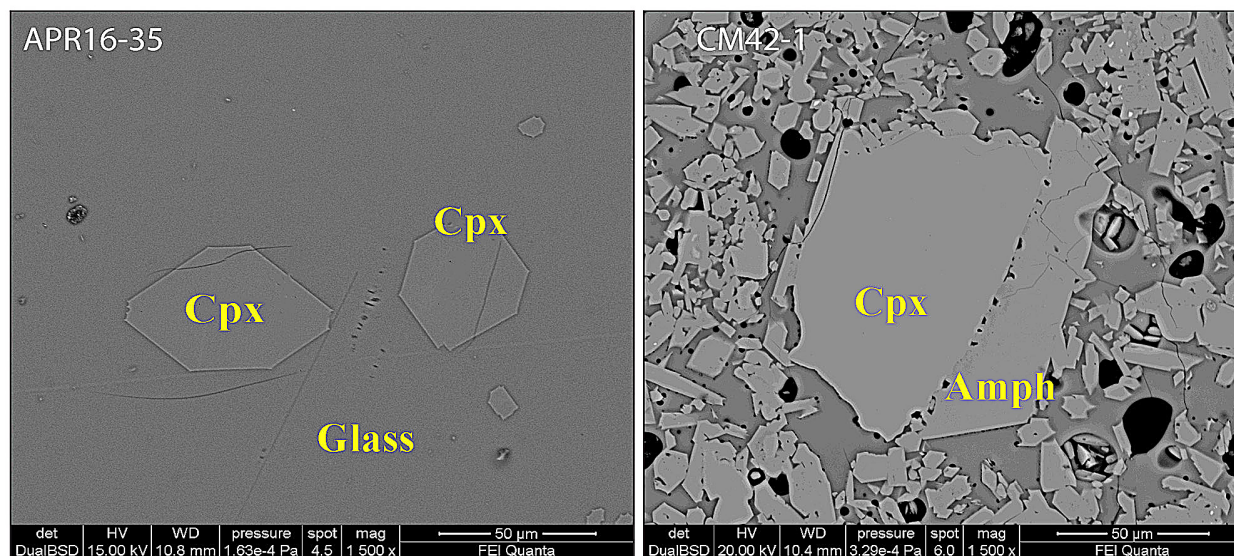
Figure 4. Backscattered SEM images of APR16-35 and CM42-1 runs; Cpx = clinopyroxene, Gl = glass.

number ($Mg\#_{0.81}$ and $Mg\#_{0.82}$ from the wet and damp run, respectively). Opx are clinoenstatites (Wo_3, En_{73}, Fs_{24}; Figure 5).

Clinopyroxene-liquid Fe-Mg exchange coefficient have been calculated by using the formula $(FeO/MgO)^{Cpx}/(FeO/MgO)^{Liq}$; the average value is 0.31±0.05 for APR16 and 0.29±0.01 for CM42 runs, taking into account FeO as FeO_{tot}. APR16 K_D values are in agreement with experimental data for hydrous basaltic compositions (0.27 ±0.06, Pichavant et al., 2014; 0.26-0.31, Sisson and Grove,
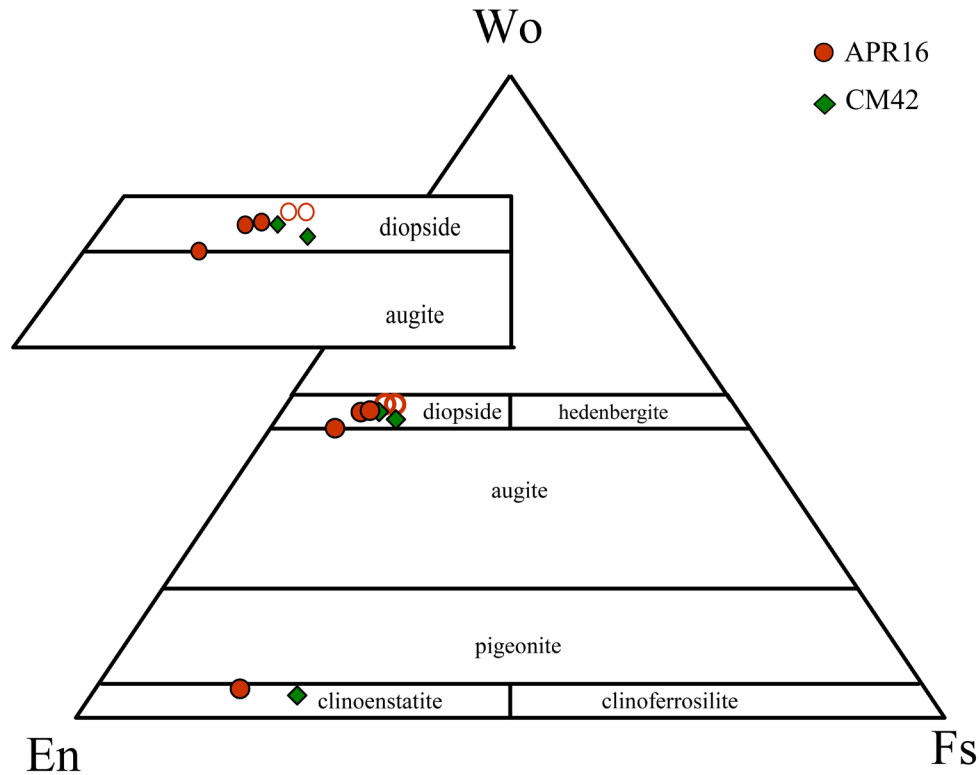
Figure 5. Pyroxene compositions plotted into the pyroxene classification diagram (Morimoto et al., 1988). Wo: wollastonite; En: enstatite; Fe: ferrosilite. Empty symbols refer to NWA experiments.

1993; 0.29±0.08, Pichavant and Macdonald, 2007). Even orthopyroxene-liquid Fe-Mg exchange coefficient has been calculated using the formula $(FeO/MgO)^{Opx}/(FeO/MgO)^{Liq}$; the average value is 0.27±0.01 for APR16 and 0.26 for CM42.

Plagioclases

Plagioclase compositions are plotted in the albite-orthoclase-anorthite ternary diagram (Figure 6). Plg from APR16 runs shows decreasing anorthite (An) content from 71 (bytownite) to 66 (labradorite) with temperature decreasing from 1000 °C to 975 °C (Table S4). Plg from the CM42 damp run is bytownite (An_{84}).

Amphiboles

In both APR16 and CM42 experiments, amphibole crystallizes when H_2O_i=5 wt%. According to the classification scheme of Hawthorne and Oberti (2007) the amphiboles are pargasite (APR16-W13, 1000 °C run) and magnesiohastingsite (CM42-2, 1050 °C run). Pargasite is characterized by $Mg\#_{0.75}$ and 1.11 wt% K_2O, whereas magnesiohastingsite shows $Mg\#_{0.70}$ and 0.67 wt% K_2O (Table S5).

Oxides

Oxides in APR16 experiments vary in composition from Cr-rich spinel [Cr#=0.46-0.44 calculated as $Cr^{3+}/(Cr^{3+}+Al^{3+})$] to Ti-magnetite with 24-28 mol% of ulvöspinel content (Usp; Table S6). Similarly, oxides from CM42 products correspond to Usp_{28-32} Ti-magnetites showing a negative correlation between Usp and H_2O_i: Usp increasing from 28 to 32 with H_2O_i decreasing from 5 to 2 wt%.

Glass

In the Total Alkali-Silica (TAS) diagram (Figure 7) the composition of residual glass (Table S7) in APR16 experiments evolves from basalt to trachybasalt with Mg#=0.62 and Na_2O/K_2O=1.85 in the NWA run at 1225 °C, to shoshonite with Mg#=0.56 and Na_2O/K_2O=1.63 in the hydrous run at 1050 °C. In turn, the chemical composition of residual glass in CM42 experiments varies from basaltic with Mg#=0.52, Na_2O/K_2O=1.81 and H_2O_f (final water content) ≈7 wt% in the hydrous run, to basaltic andesite with Mg#=0.45, Na_2O/K_2O=0.88 and H_2O_f ≈5 wt% in the damp run.

The important crystallization of plagioclase (~22 vol%) in the damp run is responsible for the relative enrichment
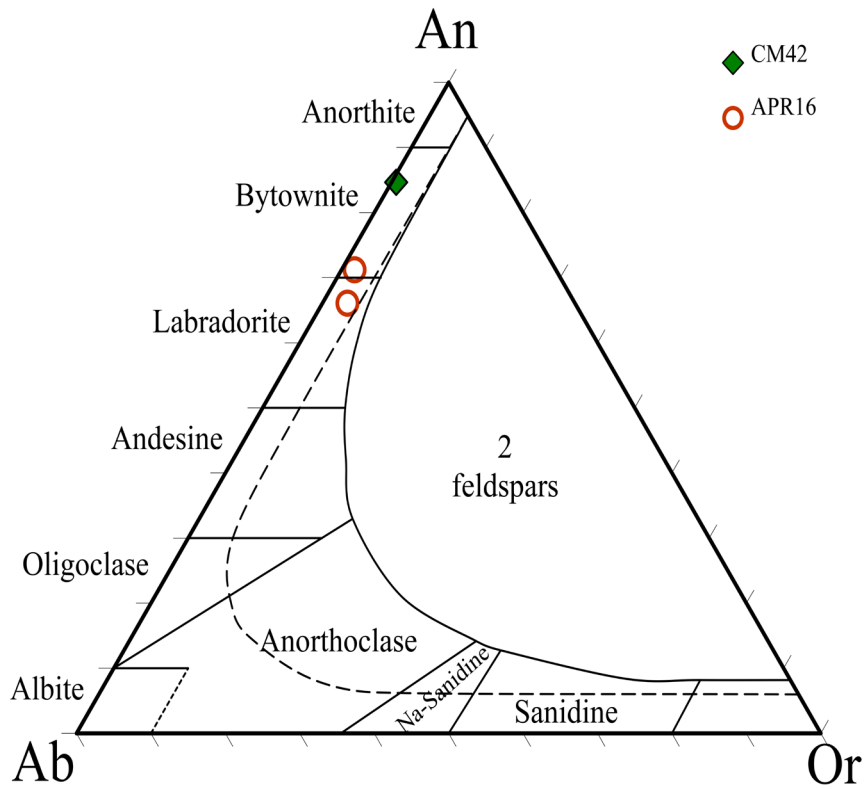
Figure 6. Feldspar compositions plotted in the Ab: albite; Or: orthoclase; An: anorthite classification diagram. Dashed line represent the solvus at 750 °C, P_{H_2O} = 100 MPa (Seck, 1971).
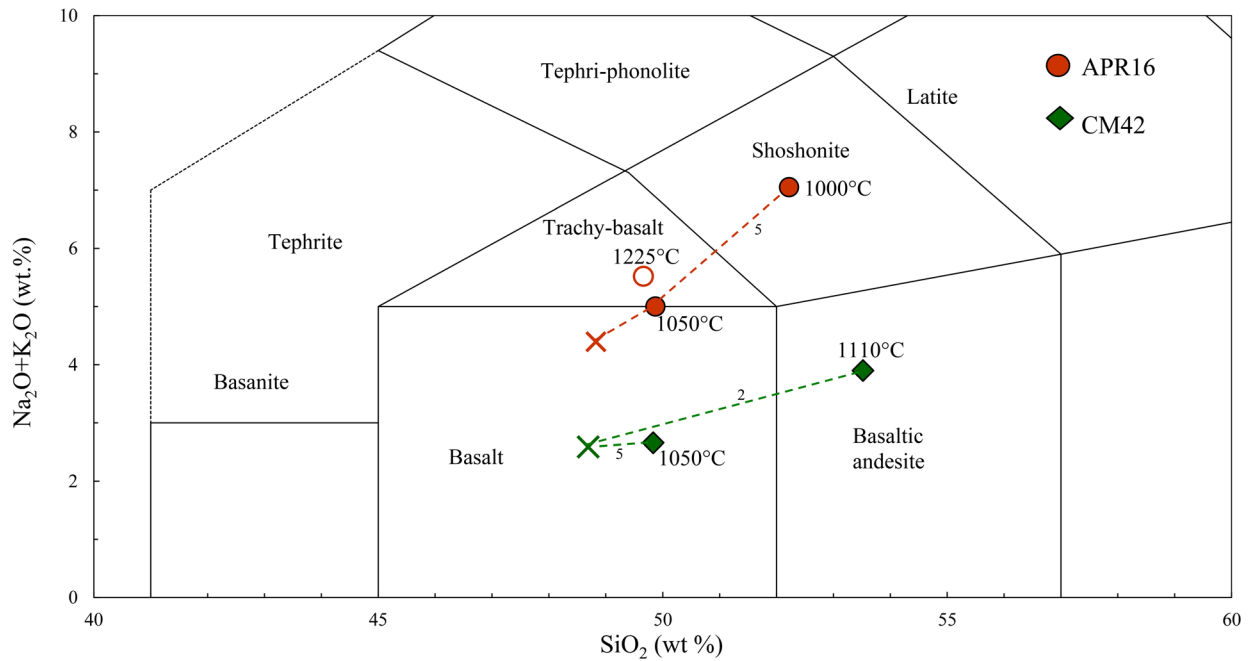
Figure 7. Composition of the APR16 and CM42 experimental glasses reported in the TAS diagram; crosses indicate starting material. Damp (2 wt% H_2O_i) and wet (5 wt% H_2O_i) runs are indicated by the numbers near to the dashed lines.

of K_2O over Na_2O in the melt, reflected by the striking decrease of Na_2O/K_2O ratio (from 2.08 of starting material to 0.88 wt%).

Rhyolite-MELTS results

The phase equilibria predicted by Rhyolite-MELTS for APR16, CM42 and MF are shown in the T-H_2O diagrams of Figure 8.

The anhydrous liquidus of APR16 is calculated at 1320 °C and decreases to 1148 °C with increasing water content to 7 wt% H_2O_i (Figure 8a). Clinopyroxene is the liquidus phase at 0-3 wt% H_2O_i, followed by oxide, orthopyroxene and plagioclase at lower temperatures. This mineral assemblage represents the stable paragenesis at H_2O contents in the residual melt lower than ~6 wt%. Olivine is the first mineral to crystallize at >3 wt% H_2O_i (Figure 8a), followed by clinopyroxene and oxides. The Ol+Cpx+Ox paragenesis is stable until, at peritectic, olivine starts to react with the melt to form orthopyroxene (Figure 8a). Amphibole crystallization is predicted by Rhyolite-MELTS calculations at temperatures <970 °C and with >5 wt% H_2O in the residual melt. Phlogopite is the last mineral to crystallize at temperatures ≤900 °C and H_2O_f ≥6 wt%. Under such conditions, the stable paragenesis consists of Gl+Opx+Cpx+Amph+Phlog+Ox (Figure 8a).

As regards CM42 composition, the liquidus temperature at anhydrous conditions is found to be at 1340 °C and rationally decreases at 1180 °C with increasing of water content to 6 wt% H_2O_i (Figure 8b). Orthopyroxene represents the liquidus phase at <3 wt% H_2O_i, followed by clinopyroxene, oxide and plagioclase at lower temperatures. Gl+Cpx+Plg corresponds to the stable paragenesis at H_2O contents in the residual melt lower than ~4 wt%. Olivine is the first mineral to crystallize at ≥3 wt% H_2O_i, followed by clinopyroxene and oxides. The Ol+Cpx+Ox paragenesis is stable until the onset of olivine-melt peritectic reaction to produce orthopyroxene, comparably to results from APR16 simulations previously described. Amphibole crystallization is retrieved by Rhyolite-MELTS at temperatures <960 °C and with H_2O-contents in the residual melt between 11 and 14 wt%. At such conditions, the stable mineral assemblage consists of Opx+Cpx+Ox+Amph.

The MF anhydrous liquidus is predicted at temperature of 1385 °C and it decreases to 1250 °C with increasing water content to 7 wt% H_2O_i (Figure 8c). Clinopyroxene is the liquidus phase at 0-1 wt% H_2O_i, followed by olivine, spinel and leucite during cooling and crystallization (H_2O_f = 0-3.5 wt%). The modelled crystallization sequence at >1 wt% H_2O_i is Ol → Ol+Cpx → Ol+Cpx+Ox → Ol+Cpx+Ox + phlogopite (Phlog). The onset of phlogopite occurs at temperatures < 1150 °C and with >3 wt% H_2O

in the residual melt. Garnet (Gt) also crystallizes and coexists with Cpx+Ox+Phlog at temperatures ≤1035 °C and ≥3.5 wt% H_2O_f.

DISCUSSION

In the following section, we discuss the phase relations of primitive subalkaline to alkaline APR16, CM42 and MF compositions combining the results of the Rhyolite-MELTS simulations with those of experiments from both this study and literature (i.e., Conte et al., 2009). We therefore address the effect of alkali content, in particular of the Na_2O/K_2O ratio, on the stability of amphibole and phlogopite.

Phase relations in the APR16, CM42 and MF composition

We find that results from Rhyolite-MELTS modelling on the alkaline basalt APR16 are in substantial harmony with experimental phase equilibria. Indeed, we observe a good correspondence between predicted models and observed phase relations from both the NWA experiment at 1225 °C (APR16-20 run) and the hydrous (~5 wt% H_2O_i) experiment at 1000 °C (APR16-W13 run; Table 1). In detail, the NWA assemblage of Gl (~1 wt% H_2O_f) +Cpx at 1225 °C is well simulated by Rhyolite-MELTS particularly when the calculations are performed using an initial water content similar to the APR16 L.O.I. value (0.61 wt%; Figure 8). In turn, for hydrous experiments the paragenesis of Gl (~7 wt% H_2O_f)+Cpx+Amph+Opx+Ox at T=1000 °C is modelled by Rhyolite-MELTS at slightly lower temperature (~970 °C; Figure 8a). At lower temperatures, olivine is unstable and replaced by Opx (Figure 8). Notably, experiments and Rhyolite-MELTS calculations show that orthopyroxene crystallizes in the APR16 magma at H_2O-rich conditions (≥5 wt% in the melt). This unexpected result indicates that at high pressure, hydrous conditions the phases driving the liquid line of descent of the primitive magmas of the Phlegrean Fields could be different from those modelled at lower pressure (e.g. Fowler et al., 2007).

The subalkaline basaltic composition of CM42 shows a higher degree of mismatch between experimental and Rhyolite-MELTS results (Figure 8b). While the paragenesis of the damp run (~2 wt% H_2O_i) at 1110 °C (CM42-2; Table 1) is Gl (~5 wt% H_2O_f)+Cpx+Ol+Opx+ Plg+Ox, that computed by Rhyolite-MELTS is Gl+Cpx+Opx+Ox. Analogously, the paragenesis of the wet run (~5 wt% H_2O_i) at the 1050 °C run (CM42-1) is Gl (~7 wt% H_2O_f)+Cpx+Ol+Amph+Ox, whereas that predicted by Rhyolite-MELTS modelling is Opx+Cpx+ Ox+Amph at temperatures <960 °C and with H_2O-contents in the residual melt between 11 and 14 wt%. The coexistence of Ol and Opx is never predicted for CM42 basalt at any of the T-H_2O conditions investigated.

PM
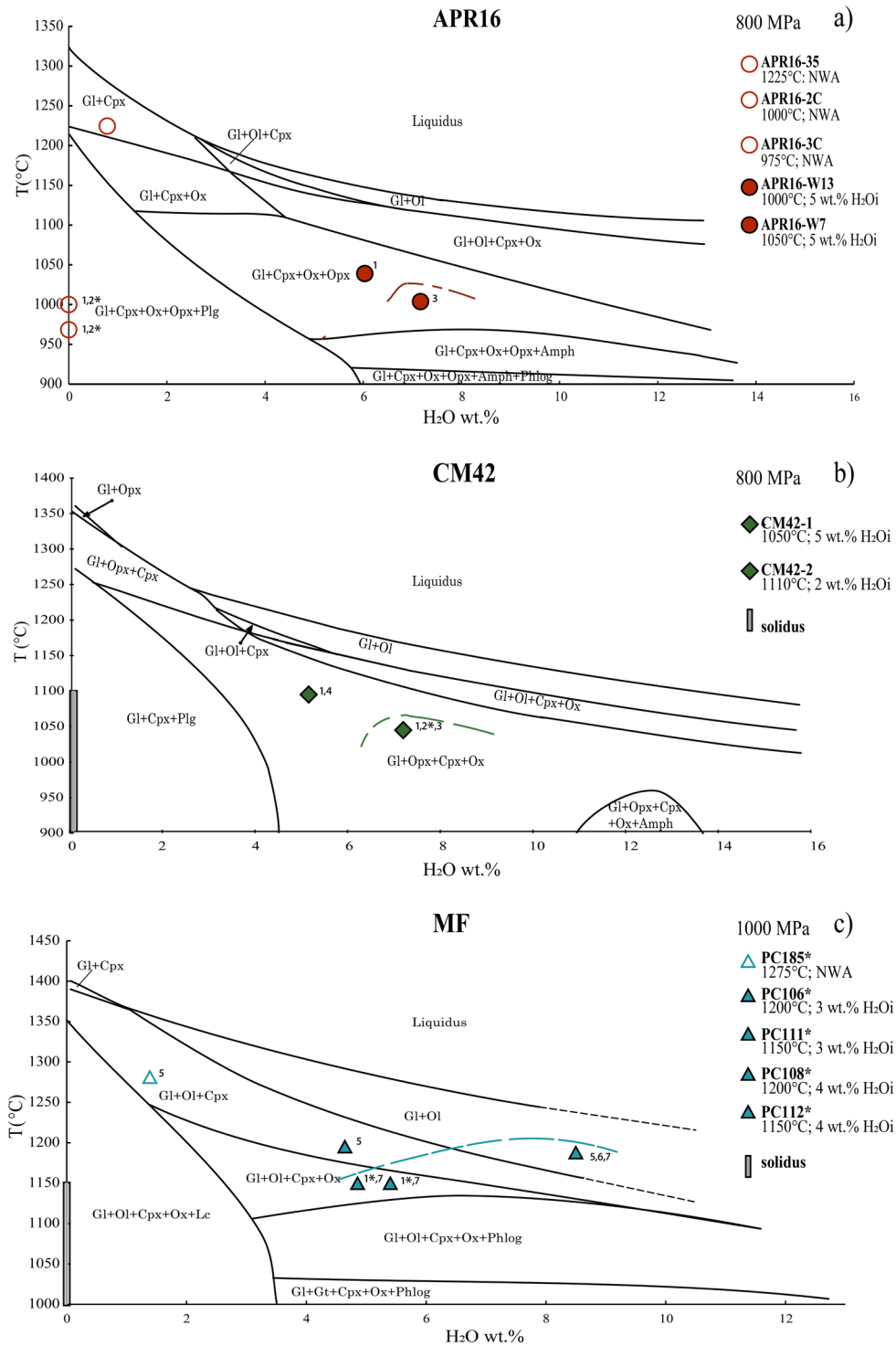
Figure 8. T (°C) vs H_2O_f (i.e. H_2O in the melt phase) diagrams showing the phase relations at P = 800 MPa for APR16 (a) and CM42 (b) compositions and P = 1000 MPa for MF (c) composition obtained by means of the Rhyolite-MELTS calculations. The diagrams also display the data obtained from the piston cylinder experiments; dashed lines represent the amphibole/phlogopite saturation curves extrapolated from the experimental data. Numbers near symbols indicate phases crystallized in the experiments but not predicted by Rhyolite-MELTS modelling: 1=Ol, 2=Opx, 3=Amph, 4=Plg, 5=Ox, 6=Cpx, 7=Phlog. 1*=absence of Ol in experimental runs; 2*=absence of Opx in experimental runs. The asterisk (*) indicates data from Conte et al. (2009). Amph: amphibole, Cpx: clinopyroxene; Gl: glass; Lc: leucite; Ol: olivine; Opx: orthopyroxene, Ox: oxide, Phlog: phlogopite, Plg: plagioclase.

PM

Moreover, Rhyolite-MELTS yields Plg crystallization exclusively when the H_2O_i in the system is lower than or equal to 3 wt% and T=1110 °C.

As regards the basanite composition of MF, phase relations modelled by Rhyolite-MELTS are fully consistent with experimental results of Conte et al. (2009; Figure 8c). In the anhydrous run at 1275 °C (PC185) and in the hydrous run (3 wt% H_2O_i) at 1200 °C (PC106) the glasses (1.6 and 4 wt% H_2O_f, respectively) are at equilibrium with Ox, Ol and Cpx. Rhyolite-MELTS is unable to predict the Ox crystallization at experimental conditions of PC106 run (T=1200 °C; 3 wt% H_2O_i); this may be due to the fO_2 imposed for calculations. Further differences concern the temperatures of Phlog saturation, which occurs at equilibrium with Ol+Cpx+Ox+Gl (8 wt% H_2O_f) in the charge at 1200 °C and at equilibrium with Cpx+Ox+Gl (5 wt% H_2O_f) in the charge at 1150 °C. The temperatures provided by Rhyolite-MELTS for Phlog crystallization are lower than ~100 °C (Figure 8c).

Effect of alkali on the amphibole stability

Experimental results show that amphibole crystallizes from both APR16 and CM42 in the hydrous experiments (~5wt% H_2O_i) at 1000 °C (APR16-W13) and 1050 °C (CM42-1), respectively.

In these runs, Amph is in equilibrium with a melt containing ~7 wt% H_2O_f. Conversely, in runs with lower

water content in the melt, amphibole does not crystallize (e.g., APR16-7W; Figure 9a; Table 1). This agrees with many experimental studies on similar compositions showing that at the similar P-T-H_2O-fO_2 conditions, amphibole crystallizes from liquids with H_2O contents higher than ~6 wt% (Krawczynski et al., 2012; Melekhova et al., 2015 and references therein). The most relevant differences between APR16 and CM42 amphiboles are K_2O contents (1.11 and 0.67 wt% in APR16 and CM42, respectively) and Mg# compositions (0.75 and 0.70 in APR16 and CM42, respectively). While the compositional diversity of the respective starting material (i.e., 1.52 and 0.84 wt% K_2O for APR16 and CM42 whole rocks, respectively) could explain the different K_2O contents in amphiboles, this cannot justify the aforementioned differences in Mg# (0.63 and 0.69, APR16 and CM42 whole rocks, respectively). Our experiments show that amphibole crystallizes at about 150 °C below the liquidus temperature, after olivine, pyroxenes and oxides crystallization significantly modifying the bulk chemistry of coexisting melt. In this context, identifying which chemical component exerts a primary control on amphibole stability on the base of starting material compositions is not straightforward (Figure 8a-c). However, some considerations can be attempted as follows. Interestingly, we find that amphibole crystallizing at higher temperature (i.e., 1050 °C; Figure 9b) is in equilibrium with a melt (i.e.,
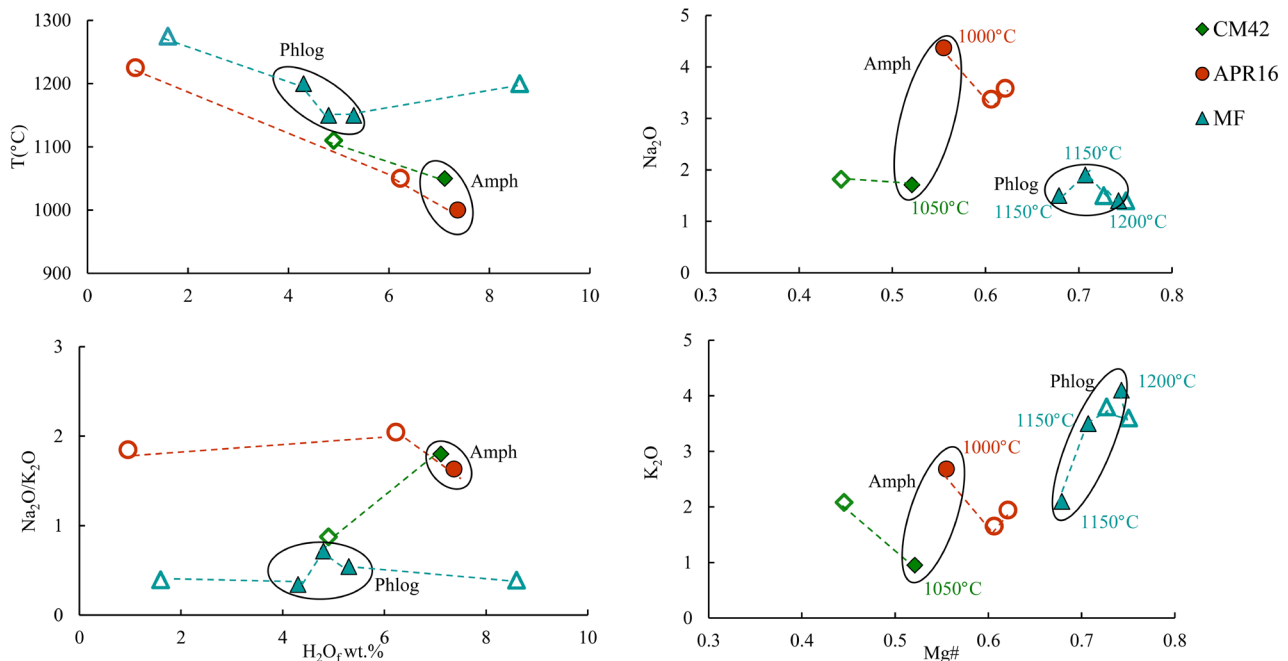
Figure 9. Experimental glasses of the samples APR16, CM42 and MF reported in the T °C vs H_2O_f (a), Na_2O vs Mg# (b), Na_2O/K_2O vs H_2O_f (c) and K_2O vs Mg# (d) diagrams.

CM42-1 melt) characterized by a lower Mg# and sodium content (Mg#$_{0.52}$ and Na$_2$O $\approx$2 wt%) with respect to that crystallizing at lower temperature (i.e., 1000 °C; Figure 9a) from APR16-W13 melt (Mg#$_{0.56}$ and ~4 wt% Na$_2$O). Despite the activity of sodium is generally considered of paramount importance for amphibole stability in arc magmas (e.g. Cawthorn and Ohara, 1976; Martin, 2007; Nandedkar et al., 2014 and references therein), our experiments, according to those realized on similar compositions (e.g., Pilet et al., 2010 and Melekhova et al., 2015), underline that the increase of Na$_2$O/K$_2$O ratio (up to 2.04 in our experiments; see Table S8 for comparison with literature data) is actually more effective in stabilizing amphibole than the absolute sodium content in the melt. The diagrams in Figure 9a-c show that the amphibole crystallization at 1050 °C in the CM42 magma is associated with the increase of water and Na$_2$O/K$_2$O ratio, but not with the variation of sodium content in the melt. Pilet et al (2010) show that K$_2$O in amphiboles increases with increasing Mg# and/or temperature. High temperature would indeed promote the increase of K$_2$O accompanied by a decrease of Na$_2$O (and then a decrease of Na$_2$O/K$_2$O ratio), due to an isostructural exchange of K for Na in the A site of amphibole. On the other hand, the increasing Fe component in the amphibole would favor the Na substitution (increase Na$_2$O/K$_2$O ratio in Amph). Thus, we consider the effects of liquid composition (i.e., degree of differentiation) to prevail on those of temperature for our amphiboles crystallized at constant pressure, as suggested by Pilet et al. (2010). The comparison of phase relations obtained at 800 MPa on the CM42 composition with those obtained with both Rhyolite-MELTS modelling and experiments on the MF leucite-basanite composition (Figure 8c), confirms that Na$_2$O/K$_2$O ratio in magmas plays a role on amphibole stability. According to Rhyolite-MELTS, amphibole never crystallizes from the MF (Figure 8c), irrespective of the absolute amount of sodium in the melt. Experimental glasses reported by Conte et al. (2009) for the 1000 MPa hydrous experiments on the MF show Na$_2$O contents comparable to those obtained in the present study on CM42 (Na$_2$O $\approx$2 wt%; Figure 9b), however, their Na$_2$O/K$_2$O ratios are lower than ours (<0.8 compared to $\geq$0.9, respectively; Figure 9c). Thus, the near-primary ultrapotassic character of the MF composition (high Mg#=0.75) favors the early crystallization (i.e. at 1200 °C) of phlogopite rather than amphibole in the experimental runs.

On the other hand, the occurrence of amphiboles in the lava flows of the Colli Albani Volcanic District (6-11 wt% K$_2$O; Gaeta and Freda, 2001; Gozzi et al., 2014; Gaeta et al., 2016) indicates that the inhibition of amphibole crystallization in ultrapotassic magmas is not caused by the high activity of potassium but, according to our experiments, it depends on the low Na$_2$O/K$_2$O ratios of magmas.

CONCLUSIONS

An alkaline (sample APR16) and a calc-alkaline (sample CM42) primitive basaltic liquids from the Phlegraean Volcanic District (South Italy) and the Capo Marargiu Volcanic District (Sardinia, Italy) are experimentally crystallized at deep crustal pressures under hydrous conditions. The experiments aim to investigate the effects of alkali on the stability of amphibole during the early stages of fractionation in alkaline/calc-alkaline magmas. Clinopyroxene is always present; orthopyroxene crystallizes in the calc-alkaline composition for H$_2$O contents <5 wt% and, unexpectedly, it also occurs in the alkaline composition. Amphibole stability is achieved in the calc-alkaline composition at 1050 °C and >5 wt% H$_2$O in the melt, while its crystallization is restricted at lower temperature (i.e. 1000 °C) in the alkaline composition. This is unexpected by virtue of the relatively high Na$_2$O content in the experimental alkaline glasses, which is thought to favor amphibole crystallization under a wider range of physico-chemical conditions. Therefore, we interpret amphibole crystallization in our experiments as being mostly controlled by the Na$_2$O/K$_2$O ratio of the residual melt rather than by its absolute sodium content. The comparison of our results with those obtained from Rhyolite-MELTS simulations and experiments on ultrapotassic compositions from literature demonstrated at deep crustal level, the crystallization of amphibole from primitive liquids depends not only on the water contents but also on of the Na$_2$O/K$_2$O that should be $\geq$0.9.

APPENDIX

Supplemental material is available for downloading at the journal site.

REFERENCES

Allen J.C. and Boettcher A.L., 1983. The stability of amphibole in andesite and basalt at high-pressures. American Mineralogist 68, 307-314.

Alonso-Perez R., Müntener O., Ulmer P., 2009. Igneous garnet

and amphibole fractionation in the roots of island arcs: experimental constraints on andesitic liquids. Contributions to Mineralogy and Petrology 157, 541-558.

Anderson A.T., 1980. Significance of hornblende in calc-alkaline andesites and basalts. American Mineralogist 65, 837-851.

Asimow P.D. and Ghiorso M.S., 1998. Algorithmic modifications extending MELTS to calculate subsolidus phase relations. American Mineralogist 83, 1127-1132.

Barclay J. and Carmichael I.S.E., 2004. A Hornblende Basalt from Western Mexico: Water-saturated Phase Relations Constrain a Pressure-Temperature Window of Eruptibility. Journal of Petrology 45, 486-506.

Blatter D.L. and Carmichael I.S.E., 1998. Plagioclase-free andesites from Zita´cuaro (Michoaca´n), Mexico: petrology and experimental constraints. Contributions to Mineralogy and Petrology 132, 121-138.

Cawthorn R.G. and Ohara M.J., 1976. Amphibole fractionation in calcalkaline magma genesis. American Journal of Science 276, 309-329.

Conte A.M., Dolfi D., Gaeta M., Misiti V., Mollo S., Perinelli C., 2009. Experimental constraints on evolution of leucite-basanite magma at 1 and 10-4 GPa: implications for parental compositions of Roman high-potassium magmas. European Journal of Mineralogy 21, 763-782.

Davidson J., Turner S., Handley H., Macpherson C., Dosseto A., 2007. Amphibole ''sponge'' in arc crust? Geology 35, 787-790.

D'Antonio M., Civetta L., Di Girolamo P., 1999. Mantle source heterogeneity in the Campanian Region (South Italy) as inferred from geochemical and isotopic features of mafic volcanic rocks with shoshonitic affinity. Mineralogy and Petrology 67, 163-192.

De Astis G., Pappalardo L., Piochi M., 2004. Procida Volcanic History: new insights in the evolution of the Phlegraean Volcanic District (Campania Region, Italy). Bulletin of Volcanology 66, 622-641.

Devine J.D., Gardner J.E., Brack H.P., Laynet G.D., Rutherford M.J., 1995. Comparison of microanalytical methods for estimating H_2O contents of silicic volcanic glasses. American Mineralogist 80, 319-328.

Fowler S.J., Spera F.J., Bohrson W.A., Belkin H.E., De Vivo B., 2007. Phase equilibria constraints on the chemical and physical evolution of the Campanian Ignimbrite. Journal of Petrology 48, 459-493.

Gaeta M. and Freda C., 2001. Strontian fluoro-magnesiohastingsite in Alban Hills lavas (Central Italy): constraints on crystallization conditions. Mineralogical Magazine 65, 787-795.

Gaeta M., Freda C., Marra F., Arienzo I., Gozzi F., Jicha B., Di Rocco T., 2016. Paleozoic metasomatism at the origin of Mediterranean ultrapotassic magmas: Constraints from time-dependent geochemistry of Colli Albani volcanic products (Central Italy). Lithos 244, 151-154.

Ghiorso M.S. and Sack R.O., 1995. Chemical mass transfer in magmatic processes; IV, A revised and internally consistent thermodynamic model for the interpolation and extrapolation of liquid-solid equilibria in magmatic systems at elevated temperatures and pressures. Contributions to Mineralogy and Petrology 119, 197-212.

Gozzi F., Gaeta M., Freda C., Mollo S., Di Rocco T., Marra F., Dallai L., Pack A., 2014. Primary magmatic calcite reveals origin from crustal carbonate. Lithos 190-191, 191-203.

Graham C.M. and Powell R., 1984. A garnet-hornblende geothermometer: calibration, testing, and application to the Pelona Schist, Southern California. Journal of Metamorphic Geology 2, 13-31.

Grove T.L., Donnelly-Nolan J.M., Housh T., 1997. Magmatic processes that generated the rhyolite of glass mountain, medicine lake volcano, N. California. Contributions to Mineralogy and Petrology 127, 205-223.

Grove T.L., Elkins-Tanton L.T., Parman S.W., Chatterjee N., Müntener O., Gaetani G.A., 2003. Fractional crystallization and mantle-melting controls on calc-alkaline differentiation trends. Contributions to Mineralogy and Petrology 145, 515-533.

Gualda G.A., Ghiorso M.S., Lemons R.V., Carley T.L., 2012. Rhyolite-MELTS: a modified calibration of MELTS optimized for silica-rich, fluid-bearing magmatic systems. Journal of Petrology 53, 875-890.

Hammarstrom J.M. and Zen E., 1986. Aluminum in hornblende: an empirical igneous geobarometer. American Mineralogist 71, 1297-1313.

Hawthorne F.C. and Oberti R., 2007. Classification of the Amphiboles. In: Amphiboles: crystal chemistry, occurrence and healts issues. (eds): F.C. Hawthorne, R. Oberti, G. Della Ventura, A. Mottana. Reviews in Mineralogy & Geochemistry 67, 55-88.

Helz R.T., 1973. Phase relations of basalts in their melting range at P_{H_2O} = 5 kbar as a function of oxygen fugacity .1. Mafic phases. Journal of Petrology 14, 249-302.

Helz R.T., 1976. Phase relations of basalts in their melting ranges at P_{H_2O} = 5 kbar. 2. Melt compositions. Journal of Petrology 17, 139-193.

Helz R.T., 1982. Phase Relations and Compositions of Amphiboles Produced in Studies of the Melting Behavior of Rocks. Reviews in Mineralogy 9B, 279-347.

Hilyard M., Nielsen R.L., Beard J.S., Patinõ-Douce A., Blencoe J., 2000. Experimental determination of the partitioning behavior of rare earth and high field strength elements between pargasitic amphibole and natural silicate melts. Geochimica et Cosmochimica Acta 64, 1103-1120.

Holland T.J.B. and Richardson S.W., 1979. Amphibole zonation in metabasites as a guide to the evolution of metamorphic conditions. Contributions to Mineralogy and Petrology 70, 143-148.

Hollister L.S., Grissom G.C., Peters E.K., Stowell H.H., Sisson

V.B., 1987. Confirmation of the empirical correlation of Al in hornblende with pressure of solidification of calc-alkaline plutons. American Mineralogist 72, 231-239.

Holloway J.R. and Burnham C.W., 1972. Melting relations of basalt with equilibrium water pressure less than total pressure. Journal of Petrology 13, 1-29.

Holloway J.R., 1973. The System Pargasite-H_2O-CO_2: A Model for Melting of a Hydrous Mineral with a Mixed-Volatile Fluid-I. Experimental Results to 8 kbar. Geochimica et Cosmochimica Acta 37, 651-666.

Krawczynski M.J., Grove T.L., Behrens H., 2012. Amphibole stability in primitive arc magmas: effects of temperature, H_2O content, and oxygen fugacity. Contributions to Mineralogy and Petrology 164, 317-339.

Kress V.G. and Charmichael I.S.E., 1991. The compressibility of silicate liquids containing Fe_2O_3 and the effect of composition, temperature, oxygen fugacity and pressure on their redox state. Contributions to Mineralogy and Petrology 108, 82-92.

Le Bas M.J., Le Maitre R.W., Streckeisen A., Zanettin R., 1986. A chemical classification of volcanic rocks based on the total alkali-silica diagram. Journal of Petrology 27, 745-750.

Le Maitre R.W.B., Dudek P., Keller A., Lameyre J., Le Bas J., Sabine M.J., Zanettin A.R., 1989. A classification of igneous rocks and glossary of terms: Recommendations of the International Union of Geological Sciences, Subcommission on the Systematics of Igneous Rocks (No. 552.3 CLA). International Union of Geological Sciences.

Martin R.F., 2007. Amphiboles in the igneous environment. Reviews in Mineralogy and Geochemistry 67, 323-358.

Masotta M. and Keppler H., 2015. Anhydrite solubility in differentiated arc magmas. Geochimica et Cosmochimica Acta 158, 79-102.

Medard E. and Grove T.L., 2008. The effect of H_2O on the olivine liquidus of basaltic melts: experiments and thermodynamic models. Contributions to Mineralogy and Petrology 155, 417-432.

Melekhova E., Blundy J., Robertson R., Humphreys M.C.S., 2015. Experimental evidence for polybaric differentiation of primitive arc basalt beneath St. Vincent, Lesser Antilles. Journal of Petrology 56, 161-192.

Moore G. and Carmichael I.S.E., 1998. The hydrous phase equilibria (to 3 kbar) of an andesite and basaltic andesite from western Mexico: constraints on water content and conditions of phenocrysts growth. Contributions to Mineralogy and Petrology 130, 304-319.

Morimoto N., Fabries J., Ferguson A.K., Ginzburg I.V., Ross M., Seifert F.A., Zussman J., Aoki K., Gottardi D., 1988. Nomenclature of pyroxenes. American Mineralogist 62, 53-62.

Middlemost E.A., 1975. The basalt clan. Earth-Science Reviews 11, 337-364.

Müntener O. and Ulmer P., 2006. Experimentally derived high-pressure cumulates from hydrous arc magmas and consequences for the seismic velocity structure of lower arc crust. Geophysical Research Letters 33, 21.

Nabelek C.R. and Lindsley D.H., 1985. Tetrahedral Al in amphibole: a potential thermometer for some mafic rocks. Geological Society of America, Abstract Programs, (United States) 17, CONF-8510489.

Nandedkar R.H., Ulmer P., Müntener O., 2014. Fractional crystallization of primitive, hydrous arc magmas: an experimental study at 0.7 GPa. Contributions to Mineralogy and Petrology 167, 1-27.

Philpotts A. and Ague J., 2009. Principles of igneous and metamorphic petrology. Cambridge University Press.

Pichavant M. and MacDonald R., 2007. Crystallization of primitive basaltic magmas at crustal pressures and genesis of the calcalkaline igneous suite: experimental evidence from St Vincent, Lesser Antilles arc. Contributions to Mineralogy and Petrology 154, 535-558.

Pichavant M., Scaillet B., Pommier A., Iacono-Marziano G., Cioni R., 2014. Nature and evolution of primitive Vesuvius magmas: an experimental study. Journal of Petrology 55, 2281-2310.

Pilet S., Ulmer P., Villiger S., 2010. Liquid line of descent of a basanitic liquid at 1.5 GPa: constraints on the formation of metasomatic veins. Contributions to Mineralogy and Petrology 159, 621-643.

Prouteau G. and Scaillet B., 2003. Experimental constraints on the origin of the 1991 pinatubo dacite. Journal of Petrology 44, 2203-2241.

Ridolfi F., Renzulli A., Puerini M., 2010a. Stability and chemical equilibrium of amphibole in calc-alkaline magmas: an overview, new thermobarometric formulations and application to subduction-related volcanoes. Contributions to Mineralogy and Petrology 160, 45-66.

Ridolfi F. and Renzulli A., 2012. Calcic amphiboles in calc-alkaline and alkaline magmas: thermobarometric and chemometric empirical equations valid up to 1,130°C and 2.2 GPa. Contributions to Mineralogy and Petrology 163, 877-895.

Rutherford M.J. and Devine J.D., 1988. The May 18, 1980, eruption of Mount St. Helens 3. Stability and chemistry of amphibole in the magma chamber. Journal of Geophysical Research 93, 949-11, 959.

Seck H.A., 1971. Koexisterend Alkali-feldspate und Plagioclase in System $NaAlSi_3O_8$-$KAlSi_3O_8$-$CaAl_2Si_2O_8$ bei temperature von 650 °C bis 900 °C. Neues Jahrbuch für Mineralogie-Abhandlungen 155, 315-395.

Sisson T.W. and Grove T.L., 1993. Experimental investigations of the role of H_2O in calc-alkaline differentiation and subduction zone magmatism. Contributions to Mineralogy and Petrology 113, 143-166.

Tecchiato V., Gaeta M., Mollo S., Perinelli C., Scarlato P., 2015. High porphyritic calc-alkaline basalts from the Cenozoic Capo

Marargiu Volcanic District (Sardinia, Italy). Goldschmidt Conference, 16-21 August, Prague, Czech Republic.

Toplis M.J., 2005. The thermodynamics of iron and magnesium partitioning between olivine and liquid: criteria for assessing and predicting equilibrium in natural and experimental systems. Contributions to Mineralogy and Petrology 149, 22-39.

Weaver S.L., Wallace P.J., Johnstonm A.D., 2013. Experimental constraints on the origins of primitive potassic lavas from the Trans-Mexican Volcanic Belt. Contributions to Mineralogy and Petrology 166, 825-843.

PM